Two-dimensional Maxwell-Bloch simulation of quasi-π-pulse amplification in a seeded XUV laser

O. Larroche*
CEA DIF, Bruyères le Châtel, 91297 Arpajon Cedex, France

A. Klisnick
ISMO, CNRS, Université Paris-Sud, 91405 Orsay Cedex, France

(Received 9 July 2013; published 5 September 2013)

The amplification of high-order-harmonics (HOH) seed pulses in a swept-gain XUV laser is investigated through numerical simulations of the full set of Bloch and two-dimensional paraxial propagation equations with our code COLAX. The needed atomic data are taken from a hydrodynamics and collisional-radiative simulation in the case of a Ni-like Ag plasma created from the interaction of an infrared laser with a solid target and pumped in the transient regime. We show that the interplay of strong population inversion and diffraction or refraction due to the short transverse dimensions and steep density gradient of the active plasma can lead to the amplification of an intense, ultrashort, quasi-"π" pulse triggered by the incoming seed. By properly tuning the system geometry and HOH pulse parameters, we show that an $\simeq$10 fs, 8×10^{12} W/cm^2 amplified pulse can be achieved in a 3-mm-long Ni-like Ag plasma, with a factor of $\gtrsim$10 intensity contrast with respect to the longer-lasting wake radiation and amplified spontaneous emission.

DOI: 10.1103/PhysRevA.88.033815 PACS number(s): 42.55.Vc, 42.50.−p

I. INTRODUCTION

The possibility of amplifying ultrashort pulses (tens of femtoseconds in duration) in a plasma-based XUV laser medium has attracted much attention in the last few years. A large amount of energy, up to several millijoules [1], can be stored in inverted ions. Such a femtosecond amplification time scale would thus lead to output peak powers comparable to, or even surpassing, those of existing XUV free-electron lasers [2,3], while relying on much smaller-scale generating devices. Experimental attempts at realizing that goal have used laser-generated plasma amplifiers seeded by femtosecond pulses of high-order harmonics (HOH) injected at one end of the active medium. The plasma amplifying rod was created either from a gas [4] through optical field ionization by a high-intensity femtosecond pulse or from a solid target [5]. In the latter case, which is discussed in this paper, a hot and dense plasma (see Fig. 1) is created by a first infrared laser pulse, and then swept gain is induced by a second, traveling-wave picosecond pulse, in the frame of the so-called transient, grazing-incidence pumping scheme [6]. Population inversions are created between some excited levels of Ne-like or Ni-like ions.

However, to date, these experimental attempts have not succeeded in imparting a sufficient amount of the available energy to the short pulse, most of it being amplified under the form of a longer-lasting (picosecond) "wake" triggered by the injected pulse. This has been traced [7] to the intrinsically nonlinear, coherent processes at work in those devices, much in the same way as in conventional short-pulse laser amplifiers studied over the past decades [8,9].

More specifically, an electromagnetic pulse can be called "short" if its duration is less than the intrinsic time scales of the amplifying medium, such as the gain recovery time (usually called "T_1") and the reciprocal gain linewidth (usually called "T_2"). Standard laser theory [10,11], leading to such notions as small-signal (linear) gain and saturation intensity, assumes that the pulse duration is longer than those time scales, thus leading to a spectral width than can possibly be narrower than the gain linewidth, which results in efficient amplification of the whole pulse. In the case of interest here, where the spectral width of the injected HOH is significantly larger than the gain linewidth, only some part of that spectrum can be expected to be appreciably amplified. A way for shorter pulses to interact more efficiently with the active medium is when the pulse intensity is high enough to induce fast changes in the atomic system or, in other words, when the Rabi frequency becomes comparable to (or [8,9] larger than) the reciprocal atomic time scales. In the case discussed in this paper, that condition is marginally satisfied, as estimated below, so that a detailed investigation of the system, going beyond standard laser amplification theory, is in order.

In this paper we investigate the spatial and temporal behavior of an HOH seed pulse injected and amplified in a transient pumping Ni-like Ag XUV laser plasma. We discuss numerical simulations performed with our two-dimensional Maxwell-Bloch code COLAX, which was recently upgraded with respect to Refs. [7,12] by improving the time-dependent description of the system, as explained in more detail in the next section. In Sec. II, we briefly recall the theoretical and numerical model used [7,12] in COLAX. In Sec. III, we first discuss the main features of the temporal behavior of the investigated system in the simple case of one-dimensional amplification of short pulses, referring to classical results [8,9]. For the pure amplifier case, i.e., with no amplified spontaneous emission (ASE), an asymptotic solution is found in the form of the so-called "π pulse" [13], in which the inversion density is fully reversed through stimulated emission, thus extracting the highest possible energy into a very short radiation pulse.

We then show, by carefully analyzing the relevant parameters [14], that such behavior should indeed be expected in the present case of XUV lasers based on transient pumping in laser-created plasmas. In Sec. IV we describe two-dimensional (2D) numerical simulations of HOH pulse amplification in

*olivier.larroche@cea.fr

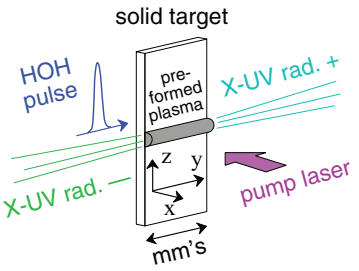

FIG. 1. (Color online) Simplified diagram of the experimental setup and coordinate axes of the theoretical and numerical model.

those systems, taking into account ASE. We show that transverse propagation effects (diffraction and refraction) play an important role in the spatial and temporal evolution of the amplified pulse, acting like an additional linear loss effect. By optimizing the parameters of the seed pulse, in particular, the incidence angle relative to the longitudinal direction, we show that it is possible to extract a significant part of the available pump energy into the amplified short pulse, which thus turns into a quasi-π pulse.

Section V gives some indications of desirable improvements to be brought to our model and to our understanding of short-pulse amplification in XUV lasers, which should help us in designing optimal short-pulse amplification experiments.

II. THEORETICAL AND NUMERICAL MODEL

The theoretical model [7,12,15–17] used to describe that situation in two-dimensional (x,y) geometry (see Fig. 1 for axes labeling) is briefly recalled in the following. The complex amplitude of the XUV field for waves propagating in the positive or negative y direction (resp. E_+ or E_-) is described in the frame of the time-envelope approximation by the paraxial propagation equation,

$$\frac{2i\omega}{c}\left(\frac{1}{c}\frac{\partial E_\pm}{\partial t} \pm \frac{\partial E_\pm}{\partial y}\right) + \frac{\partial^2 E_\pm}{\partial x^2} = -\frac{\omega^2}{c^2}(\epsilon_R E_\pm + 4\pi P_\pm), \tag{1}$$

where ω is the angular frequency of the XUV laser transition, c is the speed of light, and the residual dielectric constant

$$\epsilon_R = \frac{-\omega_p^2(x)}{\omega(\omega + i\nu_{ei})}$$

accounts for refraction through the x-dependent plasma frequency ω_p and damping of the electromagnetic waves through electron-ion collisions, with frequency ν_{ei}. It is assumed that the active plasma is sufficiently spread out in the vertical (z) direction that the hypothesis of translation invariance of the system along z holds, leading to an effectively two-dimensional (x,y) dependency only for all quantities. The time-envelope approximation is valid in the present case since the laser period $2\pi/\omega$, with a duration of a few tens of attoseconds, is much shorter than the duration of the pulse to be amplified $\tau_{\mathrm{HOH}} \sim 15$ fs.

Although the formalism described here is strictly valid only for waves that are linearly polarized along the z direction, the other polarization is not expected to behave in a much different way since the amplified XUV radiation will stay away from its critical electron density region. A more detailed discussion of polarization effects can be found in Ref. [18].

$P_\pm$, on the right-hand side of Eq. (1), is the complex amplitude of the time-enveloped polarization density, governed by

$$\frac{\partial P_\pm}{\partial t} = -\gamma P_\pm - i\frac{d^2}{\hbar}(\rho_u - \rho_l)E_\pm + \Gamma_\pm, \tag{2}$$

where γ is the dipole-dephasing rate, d is the dipole operator matrix element between the laser transition states, and the stochastic term $\Gamma_\pm(x,y,t)$ models spontaneous emission [12]. The population densities, including those of the upper and lower states of the laser transition ρ_u and ρ_l, are governed by

$$\frac{\partial \rho_i}{\partial t} = (\delta_{iu} - \delta_{il})\frac{1}{2\hbar}\mathrm{Im}(P_+E_+^* + P_-E_-^*) + \gamma_{ij}\rho_j + R_i. \tag{3}$$

Equations (2) and (3) assume the same value of the transition frequency ω for all ions; in other words, that inhomogeneous broadening can be neglected. This might be justified because the typical value of Doppler broadening, taking into account the ion temperature in the gain region, $\Delta\omega_D \sim 10^{13}$ s^{-1}, is of the same order of magnitude as γ (see below and Table I), which is responsible for homogeneous broadening. In addition, a recent careful analysis of the broadening mechanisms [19] demonstrates that Doppler broadening acts in a partly homogeneous way under the effect of ion-ion collisions.

The relevant atomic quantities, namely, γ, the pumping population fluxes R_i, and the excitation or decay rates γ_{ij} are taken from an outside hydrodynamics and collisional-radiative simulation (see Fig. 2) done with the EHYBRID code [20] in the case of Ni-like Ag [21]. EHYBRID is a 1D Lagrangian code yielding quantities as a function of x and t (see Fig. 1), also taking into account the transverse (z) expansion of the plasma. The results from EHYBRID are dependent on the

TABLE I. Calculated homogeneous (collisional, $\Delta\lambda_H$) and inhomogeneous (Doppler, $\Delta\lambda_D$) linewidths (taken from [19]) for parameter values at various relevant places in the Ag plasma under study. Linewidths in Å are given as functions of the electron density n_e in cm^{-3}, electron (T_e) and ion (T_i) temperatures in eV, together with the corresponding adiabatic small-signal gain G_0 in cm^{-1}.

n_e	T_e	G_0	T_i	$\Delta\lambda_H$	$\Delta\lambda_D$	$\Delta\lambda_H/\Delta\lambda_D$
2×10^{20}	350	60	100	5.02×10^{-3}	1.03×10^{-2}	0.49
9×10^{20}	390	400	80	2.09×10^{-2}	9.24×10^{-3}	2.27
9×10^{20}	300	180	80	2.23×10^{-2}	9.24×10^{-3}	2.41
9×10^{20}	220	60	70	2.40×10^{-2}	8.64×10^{-3}	2.78

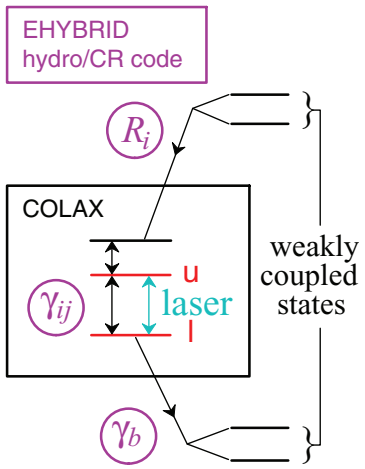

FIG. 2. (Color online) Input of atomic data into the Maxwell-Bloch code.

reduced time $t - y/c$ (instead of t alone) to model the swept gain induced by traveling-wave pumping.

The notation used here is related to notions of classical laser theory: the total dipole dephasing time $T_2 = \gamma^{-1}$ and the inversion recovery time T_1, which can be taken as the reciprocal of the largest eigenvalue of the rate matrix $[\gamma_{ij}]$. Typical values for those quantities in the present case are $T_2 \sim T_1 \sim 0.07 - 1$ ps.

Equations (1)–(3) are discretized using a split-step, Crank-Nicholson, iterative scheme [12] in our code COLAX. The code was upgraded with respect to Refs. [7,12] to allow a fully self-consistent dynamic solution of the system, with no further approximations about the time scales involved. In Ref. [7], Eq. (2) for the polarization density was directly implemented instead of relying on an adiabatic assumption, but in Eq. (3) for the populations, the term accounting for the interaction with the field was replaced with a quasistatic saturation approximation for faster calculations. It is now implemented directly, hence with no more limitations on the accessible parameter space: specifically, the simulated time scales no longer need to be larger than the gain recovery time T_1. Some improvements were also made in the programming implementation of the code. Among other things, the spontaneous radiation injection was modified to remove spurious features at large propagation angles. Also, some degree of multithread parallelization was performed for faster execution (without ASE).

The 2D (x,y) grid uses a few thousand cells in the longitudinal (y) direction since the waves take $L/c \sim 10$ ps to propagate through the $L \sim 3$ mm plasma, whereas the time step δt must be as short as a few femtoseconds to resolve the incident pulse. The transverse (x) grid must resolve the gradient lengths in the gain region (a few micrometers). It must also be able to propagate waves with a maximum angle to the longitudinal axis imposed by refraction and diffraction. Refraction in a plasma with maximum density n_e, hence the maximum plasma frequency $\omega_p = (\frac{4\pi n_e e^2}{m_e})^{1/2}$, leads to a maximum deviation angle θ_∞ away from the plasma,

$$\frac{\omega_p^2}{\omega^2} = \frac{n_e}{n_c} \lesssim 2 \times 10^{-4} \Rightarrow \theta_\infty \sim \left(\frac{n_e}{n_c}\right)^{1/2} \lesssim 14 \text{ mrad},$$

where n_c is the critical density for the XUV radiation. The corresponding maximum transverse wave vector is

$$k_\perp \sim \frac{\omega}{c}\theta_\infty = \frac{\omega_p}{c} \lesssim 6 \times 10^4 \text{ cm}^{-1}.$$

To avoid numerical aliasing, the transverse mesh size δx should be taken smaller than $\pi/k_\perp \lesssim 0.5$ μm. For diffraction to be treated in a consistent way, the mesh should resolve the waist a of a Gaussian beam whose long-distance divergence angle is $\lesssim\theta_\infty$, namely,

$$a \gtrsim \frac{\lambda}{2\pi\theta_\infty} = \frac{1}{k_\perp},$$

where $\lambda = 2\pi c/\omega$ is the XUV laser wavelength, which is nothing but the condition just derived for refraction. Diffraction should show up in simulations when the propagation length L becomes comparable to the Rayleigh length, which implies that the beam waist

$$a \lesssim \left(\frac{\lambda L}{2\pi}\right)^{1/2} \sim 7\ \mu\text{m}$$

in the present case, which turns out to be of the order of the width of the gain region (as shown in Sec. IV).

III. RESULTS IN ONE DIMENSION AND THE π-PULSE CONCEPT

In one dimension only [neglecting transverse (x) dependencies], classical results of laser theory [10,11] are found from the "adiabatic" hypothesis, whereby a time variation of the inversion density much slower than γ is assumed, so that Eq. (2) can be Fourier transformed in time keeping $\rho_u - \rho_l$ constant. The equation for the Fourier component at angular frequency Ω, leaving the spontaneous emission term aside, then reads

$$P_\pm(\Omega) \sim \frac{1}{\Omega + i\gamma}\frac{d^2}{\hbar}(\rho_u - \rho_l)E_\pm(\Omega)$$

and a stationary convective amplification regime is found. Namely, inserting the latter expression for the polarization density into the Fourier-transformed equation (1), leaving aside transverse and dispersive terms for now, and multiplying by the complex conjugate, we obtain

$$\frac{d}{ds_\pm}|E_\pm(\Omega)|^2 = \frac{G_{\text{ad}}}{1 + \frac{\Omega^2}{\gamma^2}}|E_\pm(\Omega)|^2,$$

where

$$\frac{d}{ds_\pm} = \pm\frac{\partial}{\partial y}$$

is the derivative following the propagation of the waves and

$$G_{\text{ad}} = \frac{4\pi\omega^2}{c\gamma}\frac{d^2}{\hbar\omega}(\rho_u - \rho_l). \tag{4}$$

In the small-signal limit (when the field is not strong enough to react on the populations through absorption or stimulated emission), this leads to an exponential amplification of the waves with a gain coefficient at line center given by Eq. (4).

When the assumption of adiabatic polarization is broken, the system enters a dynamic regime where the laser amplitude

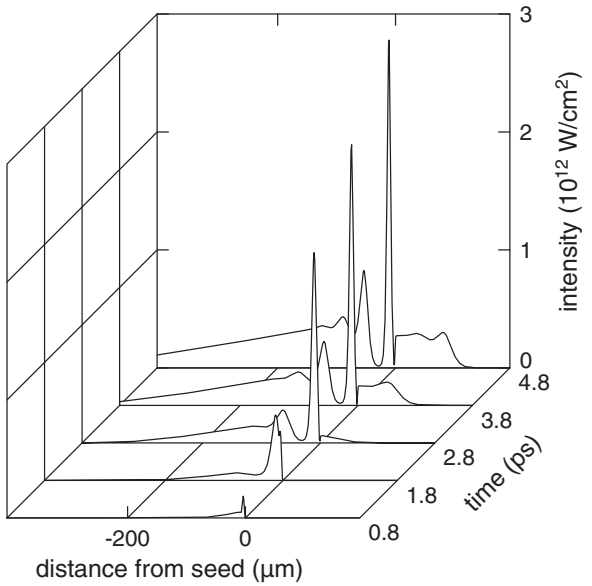

FIG. 3. One-dimensional space-time evolution of the XUV field triggered by an incoming ultrashort HOH pulse.

can display Rabi oscillations in time. As recently discussed in Ref. [14], this will occur only when the adiabatic gain $G_{\rm ad}$ is larger than a threshold value, which can be estimated from the following criterion:

$$\frac{2c}{\gamma}G_{\rm ad} > 1$$

This amounts to a comparison between the rate of amplification and the dephasing rate γ. In our case, for Ni-like Ag on the transition at $\lambda = 13.9$ nm with $\hbar\omega/d^2 \sim 2\times10^{26}$ cm^{-3} in a laser-produced plasma from a solid target, where $\rho_u - \rho_l \lesssim 1.3\times10^{17}$ cm^{-3}, strong growth should marginally prevail.

In the dynamic (strong-growth) regime with no linear damping, the above system leads to the qualitative behavior [9,15,16] displayed in Fig. 3: the incoming short pulse is only weakly amplified but, instead, generates a long-lasting, oscillatory radiation wake superposed onto an ASE background. When damping is taken into account (but without ASE), this field pattern can asymptotically evolve to a stationary propagating solitary pulse [8,13]. For small damping, that pulse causes the population inversion to be fully reversed (the Bloch vector [10] flips from upward- to downward-pointing) and is hence called a π pulse. This is also related to the so-called "area" [22] of the pulse:

$$\int \frac{d}{\hbar}E(t)dt \to \pi,$$

where $dE/\hbar$ is the Rabi frequency.

Wittke and Warter [8] investigated how and why the pulse evolves toward such an asymptotic regime. Basically, since the pulse propagates in an inverted (amplifying) medium, it keeps gathering more and more energy at a constant rate (and its width shrinks accordingly, as can be deduced from the above constant-area relationship). Hence any existing linear loss mechanism will extract an increasingly large power from the pulse, so that its amplitude cannot exceed a maximum value for which those losses exactly balance the gain from the inverted atoms. The maximum intensity that can be expected from an amplified short pulse (and its related minimum duration) can thus be estimated from the terms of that balance.

The asymptotic intensity thus depends on the values of the characteristic times for the various processes involved. The spontaneous emission time $\tau_{\rm spont} = 1/A_{\rm ul}$, where $A_{\rm ul}$ is the radiative decay rate from the upper state of the laser transition to the lower state, is ~5 ps, which is sufficiently longer than the amplification time in the dynamic regime, $\tau_{\rm dy} \sim 0.1$ ps (see Ref. [14]), for the amplified pulse wake to dominate the ASE (see Fig. 3).

However, the collisional wave damping time, with $\nu_{\rm ei} \sim 10^{13}$ s$^{-1}\Rightarrow \tau_c = \frac{2\omega^2}{\omega_p^2\nu_{\rm ei}} \sim 300$ ps, is too large to saturate the pulse growth in the way explained above [8]. This can be seen from the following simple order of magnitude estimate, neglecting transverse propagation effects. The asymptotically constant intensity $I \to I_\infty$ results from the balance between the energy collected from the fully reversed inversion density as the pulse sweeps by at the velocity of light and collisional damping:

$$\frac{dI}{dt} = \frac{2(\rho_u - \rho_l)\hbar\omega c}{\tau} - \frac{2}{\tau_c}I = 0,$$

where τ is the pulse duration. The asymptotic intensity is thus $I_\infty = (\rho_u - \rho_l)\hbar\omega c\frac{\tau_c}{\tau}$, and the length needed to reach such values is of the order of $c\tau_c$, which, in the present case, is ~90 mm, much longer than the assumed plasma length, $L = 3$ mm. The asymptotic intensity and pulse duration, from the pulse area condition $\frac{dE}{\hbar}\tau = \pi$, where E is the electric field of the pulse, would be

$$I_\infty = \frac{c}{4\pi}E_\infty^2 \quad \text{with} \quad E_\infty = \frac{\omega\tau_c}{4}d(\rho_u - \rho_l),$$

which in the present case, with the figures quoted above, is $I_\infty \approx 2.6\times10^{14}$ W/cm^2 and a pulse duration $\tau \approx 4$ fs.

The system is, nonetheless, far from the linear amplification regime since the linear amplification time, with typical gains G of hundreds of cm^{-1} (see Fig. 4), is of order $\frac{2}{Gc} \sim 0.1$ ps, much less than the transit time through the active medium, $L/c \sim 10$ ps.

However, taking into account the 2D geometry of our system with large transverse density gradients, refraction and diffraction are going to take energy out of the gain region, which constitutes an additional linear loss mechanism that might lead to a new π-pulse regime, as discussed in the next section. The latter would, in addition, be much more interesting from a practical point of view than the classical, absorption-dominated regime, since the energy pumped into the waves would then not be lost to merely heating the plasma but would, instead, be radiated outside, where it could possibly be retrieved for application use.

IV. TWO-DIMENSIONAL SIMULATIONS INCLUDING SEED AND ASE

COLAX was used to simulate the amplification of a 15-fs, 120-pJ HOH Gaussian pulse [23] with maximum intensity 10^{10} W/cm^2, incoming onto the left end of a 3-mm-long Ni-like Ag plasma, using the atomic data from EHYBRID as displayed in Fig. 4. The adiabatic small-signal gain on the

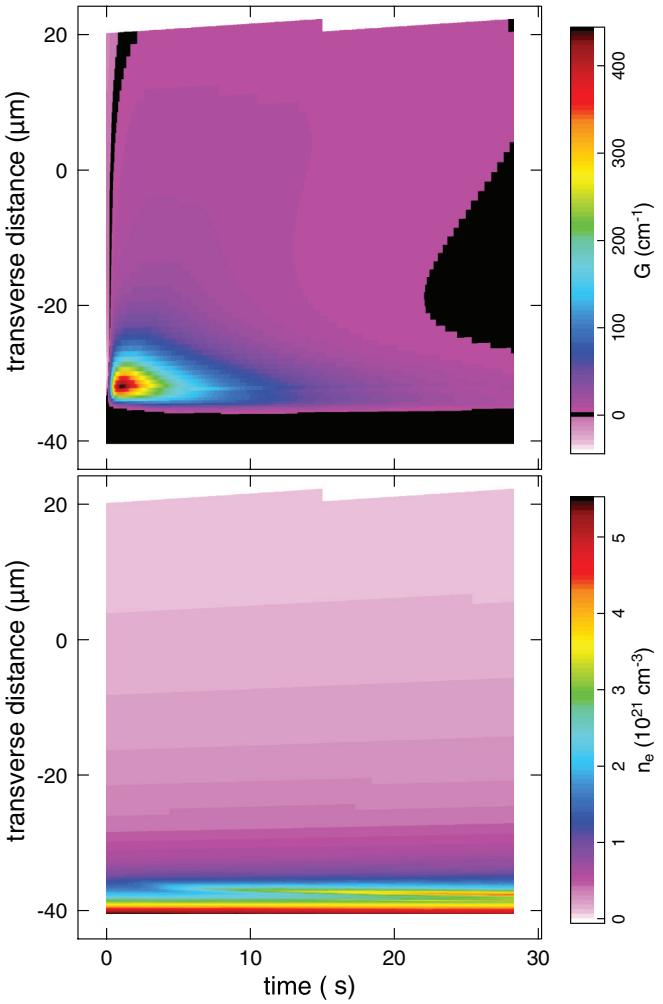

FIG. 4. (Color online) Space-time plots of the small-signal adiabatic gain coefficient G (top) and the electron density n_e (bottom) from the EHYBRID simulation of pumping in Ni-like Ag.

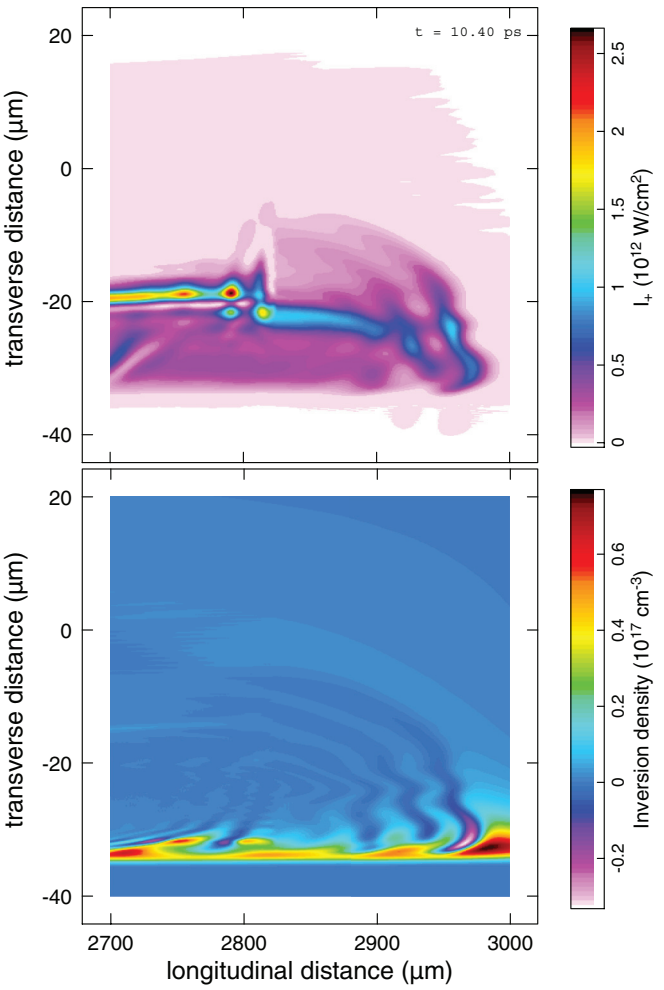

FIG. 5. (Color online) A map of the XUV intensity (top) and population inversion density (bottom) versus the transverse (x) and longitudinal (y) distances just before the pulse reaches the right end of the plasma for a nonoptimized HOH pulse. At the selected time $t = 10.4$ ps, the pulse (smeared out in the ASE) is at position $y = 2820$ μm.

$4d \rightarrow 4p$, $J = 0 \rightarrow 1$ line at 13.9 nm reaches values as high as $\sim$450 cm^{-1} (corresponding to a population inversion density $\sim 1.3 \times 10^{17}$ cm^{-3}) in a narrow region. Figure 5 displays maps of the XUV intensity and population inversion density in a 300-μm-long window just before the seed and amplified pulse reach the right end of the plasma. Here the parameters of the seed pulse (e.g., the angle of incidence) were not optimized. It can be seen that the amplified wake triggered by the seed has been refracted away from the gain region and that Rabi flipping and oversaturation are induced by ASE before the seed comes into play. The seed itself is smeared out in the ASE and amplified wake and, thus, not visible any more.

In all 2D plots in this section, starting with Fig. 4, the x-axis origin ($x = 0$) refers to the center of the COLAX simulation box, which is adjusted with respect to the data from EHYBRID to account for all relevant regions of the active plasma. The x interval displayed in the figures is the region where significant intensity values are recorded.

The fact that the amplified wave propagates away from the gain region suggests that refraction plays an important role in our system and should be investigated in more detail. The first thing to check is its effect on the HOH seed itself. In the calculation presented in Fig. 5, the seed was applied in the form of a Gaussian beam of 9-μm waist (half-width at $1/e$ in intensity), propagating at a vanishing angle with respect to the longitudinal (y) axis, and focused at $x = -32$ μm (in the reference frame of Figs. 4 and 5) onto the entry side of the plasma. To evidence more clearly the refraction of the seed, the simulation was run again with no interaction with the amplifying atomic system, but only the free-electron component, which is responsible for refraction through the x dependency of the electron density n_e as displayed in Fig. 4. The incoming signal was given a constant intensity in time instead of being in the form of a short pulse. Since the system is linear when the interaction with the atomic dipoles is turned off, this allows us to represent the whole pulse propagation in the same plot, in a way similar to a classical ray-tracing calculation except that diffraction effects are included. The intensity thus obtained is displayed in Fig. 6 at time $t = 11$ ps. The seed pulse is seen to be strongly refracted away from the gain region (located around $x = -32$ μm) after a few hundred microns of propagation in the y direction. An Airy-like

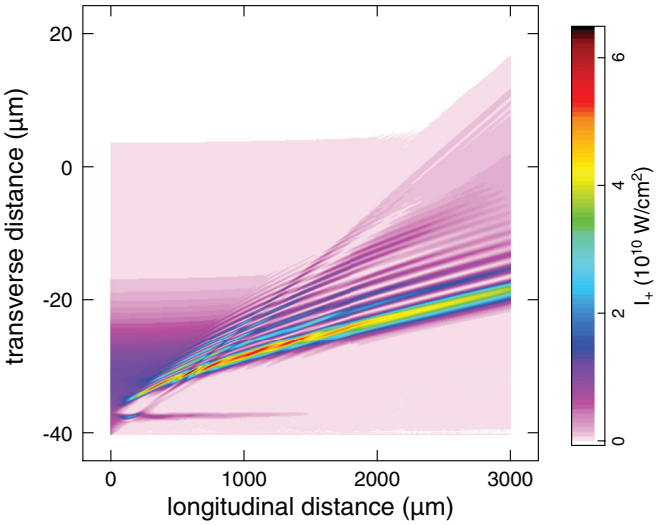

FIG. 6. (Color online) Map of the XUV intensity versus longitudinal and transverse distances just after the pulse reaches the right end of the plasma, with the interaction with bound electrons turned off. The intensity of the incoming pulse was left on at a constant value to display the whole propagation in the same graph.

interference pattern [24] is seen to build up, as expected from linear wave propagation in a medium with a transverse gradient of the refraction index. At the right end of the plasma, the main maximum of that pattern has been displaced to $x \approx -18$ μm, which is the position of the maximum amplified intensity in the full simulation (see Fig. 5). A straightforward interpretation of this fact is that the amplified signal just follows the seed and, thus, gets away from the maximum gain region too.

It is thus necessary to adjust the seed incidence angle so that the maximum of the reflection Airy pattern remains in the maximum gain region. In the present case, the best angle is found to be $\alpha \approx -8$ mrad. This is illustrated in Fig. 7.

One can see that the seed pulse now reaches the high-gain region, where it is reflected. However, due to the stronger free-electron density gradient there, the pulse is more strongly

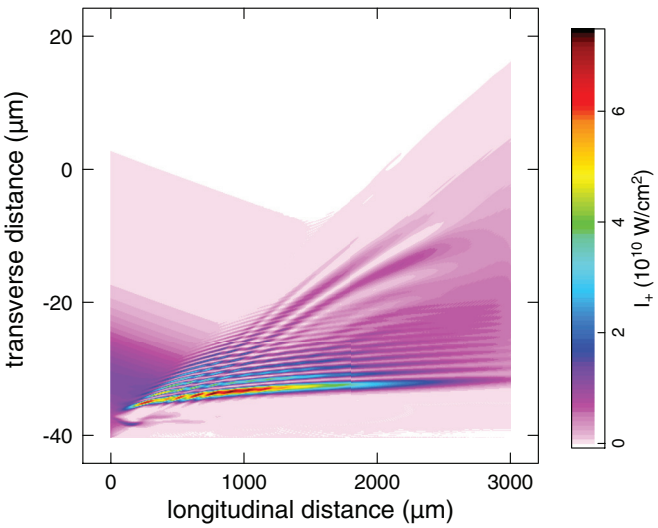

FIG. 7. (Color online) Same as Fig. 6, but with an optimized incidence angle of -8 mrad for the incoming seed pulse.

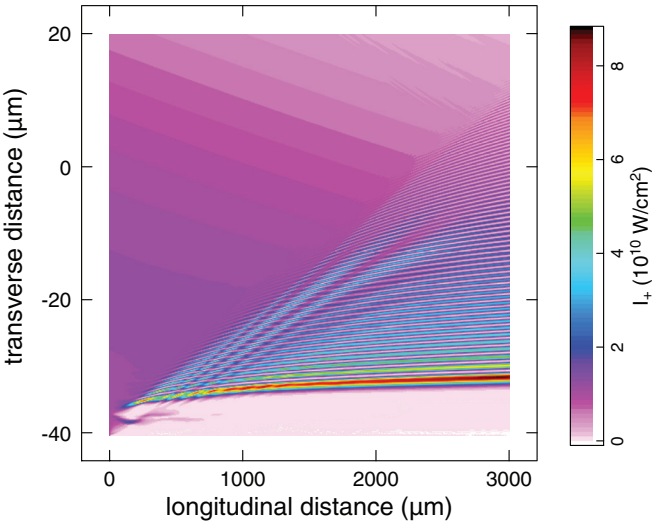

FIG. 8. (Color online) Same as Fig. 6, but with optimized geometrical parameters (incidence angle, -8 mrad; beam waist, 50 μm) for the incoming seed.

refracted than in the nonoptimized case shown in Fig. 6. Propagation in the high-gain region over the whole plasma length can still be obtained through a sustained interference between the incident and the reflected pulses. This requires a wider waist, $\sim$50 μm, hence more ($\times$25) energy is needed to maintain a given local intensity. As a trade-off, the demand for pointing accuracy is reduced. In the present case, the best shooting position, adjusted from the angle and longitudinal propagation length needed, was found to be $x = -20$ μm. The optimized propagation geometry is depicted in Fig. 8. The width Δx of the first intensity maximum near the reflection region around $x = -30$ μm in Fig. 8 ($\Delta x \approx 0.7$ μm) is consistent with the estimate for the width of the first maximum of an Airy pattern [24], given the relevant parameters, namely,

$$\Delta x = \left(\frac{\lambda^2 L_g}{4\pi^2 \sin^2 \alpha} \right)^{1/3},$$

where $L_g = n_e (dn_e/dx)^{-1}$ is the density gradient scale length in the reflection region, estimated to be a few micrometers from the density profile plotted in Fig. 4.

Using the adjusted seed geometry described above, the simulation was run again with the interaction with bound electrons turned back on. In addition, the HOH pulse injection time was also adjusted so that it starts getting amplified as soon as possible, before the ASE has had time to grow [18]. The seed was thus injected 0.5 ps earlier than in the nonoptimized case to match more closely the increase in the population inversion. Other parameters can also be tuned up, e.g., the HOH pulse intensity. The seed intensity was taken 10 times as high as in the nonoptimized case in Fig. 5, which, taking into account the larger beam waist, leads to an energy of $\sim$30 nJ in the pulse, of the same order of magnitude as the typical seed energy investigated in Ref. [15]. The result is displayed in Fig. 9, just before the pulse leaves the plasma. Compared with the unoptimized calculation displayed in Fig. 5, it can be seen that the amplified wake following the HOH pulse has been brought back into the gain region. This optimized

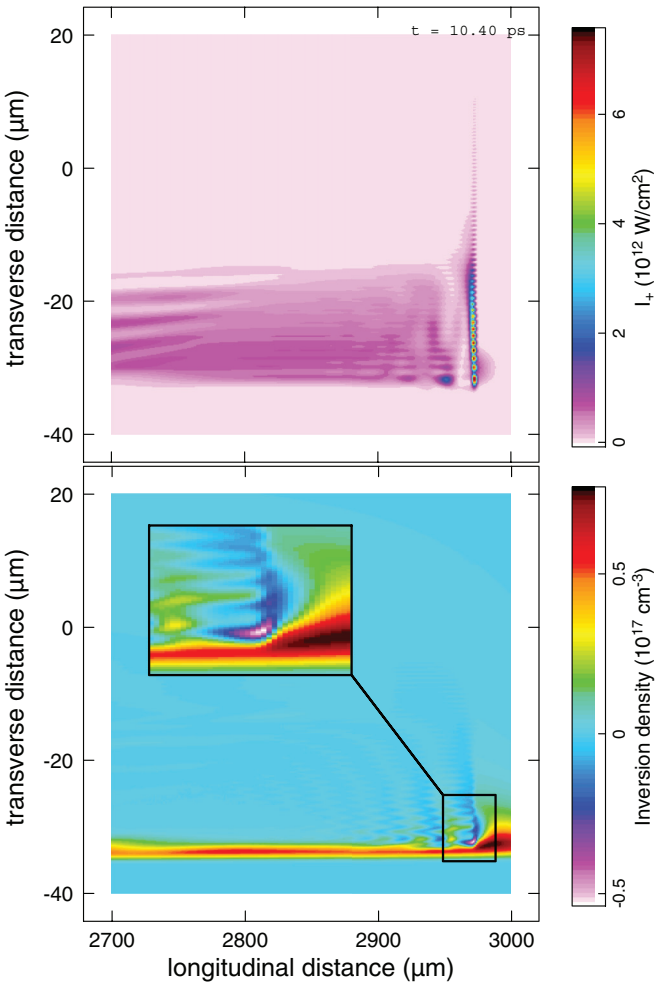

FIG. 9. (Color online) Same as Fig. 5, but for a fully optimized set of HOH pulse parameters (see text). This leads to a very intense, 10-fs pulse, which can be seen at position $y = 2970\ \mu$m at the selected time $t = 10.4$ ps. Compared with the nonoptimized case in Fig. 5, the pulse has a much higher contrast with respect to the following wake and ASE.

seeding configuration results in a very short (∼10-fs) and very intense ($\sim 8 \times 10^{12}$ W/cm^2) pulse, with a much better contrast with respect to the following wake and ASE (note that the intensity scales are different in Figs. 5 and 9). More complete Rabi flipping of the population inversion is seen to occur upon crossing of the amplified pulse, as shown in the inset in Fig. 9: the inversion density gets as low as −70% of its initial value created by pumping. However, the interference pattern of the reflected seed pulse still shows up in the transverse intensity profile of the amplified pulse. This suggests that it has not yet reached an asymptotic autonomous regime of the kind described in Ref. [8], because a self-sustaining pulse would not depend on the presence of an incoming pulse. Thus removing the incoming pulse would probably remove most of the interference features.

The geometrical optimization procedure just described can be summarized as follows. The seed incidence angle is first chosen such that its refraction turning point lies in the maximum gain region: from the electron density value n_e there (as given by the atomic physics package), the optimum incidence angle is thus

$$\alpha \approx \left(\frac{n_e}{n_c}\right)^{1/2},$$

where

$$n_c = \frac{m_e \omega^2}{4\pi e^2}$$

is the critical density for the amplified radiation with angular frequency ω. Then the seed waist w in the x direction is set such that the whole plasma length L is irradiated by the seed, namely, $w \approx \alpha L$.

V. CONCLUSION AND PROSPECTS

The two-dimensional Maxwell-Bloch code COLAX has been upgraded to include a fully dynamic treatment of the Bloch equations for the polarization and population densities. It was used to calculate the amplification of a femtosecond HOH seed in a Ni-like Ag XUV laser plasma generated from a solid target in the swept-gain, transient-pumping regime. The high gain achieved in this plasma allows the system to enter a strong-growth dynamical evolution involving Rabi oscillations. Using a 1D approximation we discuss how this system could reach an asymptotic solution leading to a self-standing π pulse, where gain from the population inversion is balanced by loss from collisional damping. When accounting for two dimensions we show that refraction in the strong transverse density gradient and diffraction actually play a major role in the spatial and temporal evolution of the system, while they can act as an additional linear loss for the amplified wave. Appropriate tuning of the HOH seed parameters, namely, pointing and focusing and injection time, is thus shown to be crucial. With optimized parameters we show that an amplified pulse of $\simeq$10 fs duration and $\simeq 8 \times 10^{12}$ W/cm^2 peak intensity can be achieved in a 3 mm-long, Ni-like Ag plasma. This pulse duration and peak intensity are orders of magnitude beyond what would be reached in the linear adiabatic amplification regime, where these quantities are controlled by the spectral bandwidth and saturation intensity, respectively. The optimized seed parameters lead to an improved intensity contrast of $\gtrsim$10 over longer-lived ASE background.

Future work will include the investigation of the effect of refraction or diffraction over longer propagation lengths, to check the feasibility of an asymptotic, truly autonomous solution. Further improvements of the code will be considered, in particular, more consistent treatment of the electromagnetic field polarization, following Ref. [18], or an extension to 3D modeling (including the z direction) that would allow a more quantitative evaluation of the achievable output pulse energy.

[1] B. Rus, T. Moček, A. R. Präg, M. Kozlová, G. Jamelot, A. Carillon, D. Ros, D. Joyeux, and D. Phalippou, Phys. Rev. A **66**, 063806 (2002).

[2] V. Ayvazyan, N. Baboi, J. Bähr, V. Balandin, B. Beutner, A. Brandt, I. Bohnet, A. Bolzmann, R. Brinkmann, O. I. Brovko *et al.*, Eur. Phys. J. D **37**, 297 (2006).

[3] E. Allaria, R. Appio, L. Badano, W. A. Barletta, S. Bassanese, S. G. Biedron, A. Borga, E. Busetto, D. Castronovo, P. Cinquegrana *et al*., Nat. Photon. **6**, 699 (2012).
[4] J.-Ph. Goddet, S. Sebban, J. Gautier, Ph. Zeitoun, C. Valentin, F. Tissandier, T. Marchenko, G. Lambert, M. Ribières, D. Douillet, T. Lefrou, G. Iaquaniello, F. Burgy, G. Maynard, B. Cros, B. Robillard, T. Moček, J. Nejdl, M. Kozlová, and K. Jakubczak, Opt. Lett. **34**, 2438 (2009).
[5] Y. Wang, E. Granados, F. Pedaci, D. Alessi, B. Luther, M. Berrill, and J. J. Rocca, Nat. Photon. **2**, 94 (2008).
[6] D. H. Martz, D. Alessi, B. M. Luther, Y. Wang, D. Kemp, M. Berrill, and J. J. Rocca, Opt. Lett. **35**, 1632 (2010).
[7] I. R. Al'miev, O. Larroche, D. Benredjem, J. Dubau, S. Kazamias, C. Möller, and A. Klisnick, Phys. Rev. Lett. **99**, 123902 (2007).
[8] J. P. Wittke and P. J. Warter, J. Appl. Phys. **35**, 1668 (1964).
[9] F. T. Arecchi and R. Bonifacio, IEEE J. Quantum Electron. QE **1**, 169 (1965).
[10] A. Yariv, *Quantum Electronics*, 3rd ed. (Wiley, New York, 1989).
[11] A. E. Siegman, *Lasers* (University Science Books, Mill Valley, CA, 1986).
[12] O. Larroche, D. Ros, A. Klisnick, A. Sureau, C. Möller, and H. Guennou, Phys. Rev. A **62**, 043815 (2000).
[13] A. G. Fox and P. W. Smith, Phys. Rev. Lett. **18**, 826 (1967).
[14] O. Larroche, L. Meng, A. Le Marec, and A. Klisnick, Opt. Lett. **38**, 2505 (2013).
[15] C. M. Kim, K. A. Janulewicz, H. T. Kim, and J. Lee, Phys. Rev. A **80**, 053811 (2009).
[16] E. Oliva, Ph. Zeitoun, M. Fajardo, G. Lambert, D. Ros, S. Sebban, and P. Velarde, Phys. Rev. A **84**, 013811 (2011).
[17] F. Tissandier, S. Sebban, J. Gautier, Ph. Zeitoun, E. Oliva, A. Rousse, and G. Maynard, Appl. Phys. Lett. **101**, 251112 (2012).
[18] C. M. Kim, J. Lee, and K. A. Janulewicz, Phys. Rev. Lett. **104**, 053901 (2010).
[19] A. Calisti, S. Ferri, C. Mossé, B. Talin, A. Klisnick, L. Meng, D. Benredjem, and O. Guilbaud, High Energy Density Phys. **9**, 516 (2013).
[20] G. J. Pert, J. Fluid Mech. **131**, 401 (1983).
[21] F. de Dortan, M. Busquet, A. Bar-Shalom, M. Klapisch, J. Oreg, B. Rus, M. Kozlová, and J. Nejdl, *X-Ray Lasers 2008, Springer Proceedings in Physics*, Vol. 130 (Springer-Verlag, Berlin, 2009), p. 231.
[22] S. L. McCall and E. L. Hahn, Phys. Rev. **183**, 457 (1969).
[23] S. Kazamias, F. Weihe, D. Douillet, C. Valentin, T. Planchon, S. Sebban, G. Grillon, F. Augé, D. Hulin, and Ph. Balcou, Eur. Phys. J. D **21**, 353 (2002).
[24] V. L. Ginzburg, *The Propagation of Electromagnetic Waves in Plasmas*, 2nd ed. (Pergamon Press, Oxford, UK, 1970).